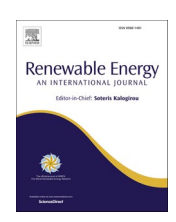


Contents lists available at ScienceDirect

# Renewable Energy

journal homepage: www.elsevier.com/locate/renene





# System identification and finite element model updating of a 6 MW offshore wind turbine using vibrational response measurements

Bridget Moynihan<sup>a</sup>, Azin Mehrjoo<sup>a</sup>, Babak Moaveni<sup>a,\*</sup>, Ross McAdam<sup>b</sup>, Finn Rüdinger<sup>b</sup>, Eric Hines<sup>a</sup>

# ARTICLE INFO

Keywords:
Offshore wind turbine
System identification
Model updating
Bayesian model updating
Digital twinning

# ABSTRACT

Offshore wind energy is playing an increasingly vital role in the clean energy transition around the world, and improved reliability of wind turbine structures is necessary for the long-term success and efficiency of renewable energy. Increased reliability would reduce costs associated with maintenance due to breakages and in turn reduce the levelized cost of energy for offshore wind energy sources. Structural health monitoring methods can be used to predict breakages and extend lifetimes by continuously monitoring instrumented structures. This paper presents system identification and model updating of a 6 MW offshore wind turbine using vibration measurements under varying operational conditions. The turbine is monopile-supported and instrumented with strain gauges and accelerometers at several elevations along the tower and monopile. Effective stiffness of soil springs in the model are updated to match modal-predicted natural frequencies and mode shapes of the first two modes with those identified from measurements at different operating conditions. A deterministic and probabilistic (Bayesian) approach to model updating are compared. The sensitivity of identified modal parameters and the updated model parameters are investigated with respect to operational and environmental conditions such as wind speed. Results show that deterministic model updating can match modal parameters with high accuracy across datasets and environmental conditions. Bayesian model updating results successfully estimate the posterior distribution of updating model parameters with an increasing degree of certainty as more data is used.

### 1. Introduction

Offshore wind (OSW) is poised to play an important role in the renewable energy portfolio of the United States, with procurement goals totaling over 39 GW by 2040 [1]. To reach state and federal OSW goals, the US will need to deploy thousands of new offshore wind turbines (OWTs) by the end of this decade [2]. While both the number and size of OWTs to be installed in US waters continue to grow, the reliability and longevity of OWT structures is increasingly crucial for the success and affordability of the clean energy transition. This reliability and longevity can be assured by effective monitoring of OWTs. This paper explores the importance of condition monitoring (CM) of OWTs in increasing its reliability through structural health monitoring (SHM) and finite element (FE) model updating.

CM offers a range of substantial benefits that directly impact the performance and longevity of these turbines. By continuously assessing the health of OWT components, CM has the potential to prevent

breakages, reduce unscheduled downtime, and significantly extend their operational lifetimes [3]. As a result, CM not only safeguards the structural integrity of OWTs but also plays a role in reducing the overall levelized cost of energy [3,4]. These methods have most commonly been deployed on gearboxes, drivetrains, and blades, with less focus on the tower and substructure (foundation) [4,5]. However, the reliability of the entire OWT structure, including the tower and substructure, is critical for the long-term viability of wind energy systems [6]. This is where SHM, a field specializing in the instrumentation and continuous monitoring of civil infrastructure, comes into play. SHM can be harnessed to comprehensively analyze OWTs, tracking the behavior of both towers and substructures. Furthermore, the instrumentation used in SHM can be strategically optimized to provide cost-effective and informative measurements, as demonstrated in prior work focused on offshore wind turbines [7,8].

Vibration-based SHM involves the collection of dynamic measurements using specialized sensors such as accelerometers or strain gauges

E-mail address: babak.moaveni@tufts.edu (B. Moaveni).

a Dept. of Civil and Environmental Engineering, Tufts University, Medford, MA, USA

<sup>&</sup>lt;sup>b</sup> Ørsted A/S, Nesa Allé 1, 2820, Gentofte, Denmark

<sup>\*</sup> Corresponding author.

[6,7,9]. These sensors are installed on parts of the structure to record vibrations in real time. In the process of system identification of an instrumented structure, the extraction of modal parameters-natural frequencies, damping ratios, and mode shapes-from vibrational response readings can be used for condition assessment or damage detection [10]. Extracted modal parameters are invaluable for condition assessment and damage detection. By comparing current modal parameters with baseline values, anomalies or deviations can be identified. Any significant changes in these parameters, such as shifts in natural frequencies or alterations in mode shapes, can signal the presence of damage within the structure [10]. Further, system identification can identify relationships between environmental conditions and the structural behavior, which must be considered in order to accurately predict damage with modal properties [11]. System identification methods are classified by three different metrics: 1) input-output (e.g. ARX) vs output only (e.g. SSI-COV and SSI-DATA); 2) parametric (e.g. ERA, NExT-ERA) vs nonparametric (e.g. peak picking); 3) frequency domain (e.g. peak picking, frequency domain decomposition) vs time domain (e.g. autoregressive methods). In the present study, the SSI-DATA method is employed, which falls under the category of output-only, parametric, and time domain techniques. The SSI-DATA [12,13] method has been explored by researchers for the continuous monitoring of structures [11] as well as offshore wind turbines [14,15].

Measurements and extracted modal parameters can then be used in the development of a digital twin (DT)—a virtual representation closely mirroring the physical structure. A digital twin functions as a dynamic, data-driven counterpart to the physical wind turbine which can be used to predict the structural response of the structure due to loading conditions, to predict breakages, or to estimate the remaining useful lifetime. DT integrates real-time data from sensors and measurements, enabling continuous monitoring and analysis of the turbine's condition and performance. This virtual model allows for the simulation of the wind turbine's behavior under varying loading conditions, providing valuable insights into its structural health. A DT can be developed through a process known as model updating. This process aims to minimize the disparity between an initial mathematical model (often a finite element model) and the actual measurements obtained from the physical turbine. Model updating involves adjusting specific model parameters, typically by matching the modal properties of the virtual model with those of the real structure [16]. Model updating is essential for offshore wind turbines to ensure accurate predictions and reliable structural assessments, as the environmental conditions and operational parameters experienced by these turbines can vary significantly [15], requiring the model to be regularly adjusted to capture these changes and improve its predictive capabilities. Model updating can be approached in two ways: deterministically [17-24], by minimizing an objective function that measures the residuals between model predictions and measurements, or through Bayesian inference [25-33], which allows for the estimation of a posterior distribution of uncertain model parameters combining prior knowledge with likelihood of observed data. These two complementary approaches offer valuable tools for maintaining the accuracy and reliability of the DT in the environmentally changing conditions of offshore wind energy systems which is aligned with the purpose of CM.

In model updating, an initial FE model is built using known properties of the OWT. In the case of monopile-supported OWTs, the soil-structure interaction at the mudline can be modeled with a variety of methods [34] which can have important effects on modeling accuracy [35,36]. The industry standard approach recommended by Det Norske Veritas - Germanischer Lloyd (DNV-GL) was originally developed using piles up to 1 m in diameter and is now considered outdated due to the growing size and increased rigidity of modern OWT monopile diameters with lower length to diameter ratios [34,37]. A more recent approach known as 'PISA' focused on large diameter monopiles with lower length to diameter ratios. The PISA approach models a macro-element at the mudline [38], and [37] showed that the macro-element can be

decomposed into equivalent lateral and rotational stiffness terms.

Many numerical studies have been done on model updating of OWT towers and foundations [39-42], however, a notable gap exists when it comes to the practical applications on operating OWTs. Previous research primarily focused on theoretical or simulated scenarios. In contrast, this study delves into the practical implementation of model updating techniques for a real 6 MW monopile-supported OWT operating in a field environment. In the literature there are a couple studies on real OWT: Nabiyan et al. [43] conducted FE model updating of a 2 MW OWT for virtual sensing of fatigue-sensitive hotspots, [44] used an extended Kalman filter to estimate input loads and FE model parameters on a jacket-supported OWT, and [45] carried out deterministic model updating on the jacket foundation of a 5 MW OWT. Most model updating of OWTs has been deterministic, and limited research has utilized batch Bayesian inference for a probabilistic approach. Recently [46], showed the value of Bayesian model updating in a numerical study of a monopile-supported OWT.

This paper conducts a two-step digital twinning of monopilesupported OWTs: system identification and FE model updating. The initial step utilizes operational measured data from a 6 MW monopilesupported OWT, instrumented with a series of accelerometers and strain gauges, in conjunction with data collected from the Supervisory Control and Data Acquisition (SCADA) system. This rich dataset, sampled at a frequency of 25 Hz over a two-week operational period, is used in the system identification process where the natural frequencies and mode shapes of the OWT are estimated. Then, a FE model is built using a simplified model for soil-structure interaction. Using the information from the first step, model updating is conducted to estimate soilstructure interaction springs. Model updating is done both deterministically and through Bayesian inference and results are compared. The operational modal analysis and deterministic model updating is performed for every 10-min window of data over the available period. The results show how the effective stiffness at the mudline changes according to environmental and operational conditions. This research distinguishes itself by addressing practical challenges in model updating for monopile-supported OWTs, incorporating probabilistic methods, considering soil-structure interaction, and utilizing real operational data. These novel elements contribute to a more comprehensive and relevant understanding of OWT structural health and behavior.

# 2. Dataset

# 2.1. Measurement channels

This paper utilizes data collected from a 6 MW monopile-supported offshore wind turbine which is owned and operated by Ørsted energy company [47]. The turbine is instrumented with a series of strain gauges and accelerometers, as well as a supervisory control and data acquisition (SCADA) system, summarized in Table 1.

Accelerometers are installed to monitor the vibration of the turbine in response to operational and environmental forces. Accelerometers are placed at 4 elevations along the height of the tower and monopile

Table 1
Measurement channels of instrumented 6 MW offshore wind turbine.

Available Data	Sampling Rate
Accelerometers (12 channels)	25 Hz
3 sensors at 4 elevations along structure	
Strain Gauges (16 channels)	25 Hz
4 sensors at 4 elevations along structure	
SCADA System (5 channels)	10 Hz
Wind Speed [m/s]	
Power Output [kW]	
Rotor Speed [rpm]	
Pitch Angle [deg]	
Yaw Angle [deg]	

structure where installation at each elevation consists of 2 orthogonal sensors placed  $135^\circ$  from global North. A third accelerometer is located  $45^\circ$  from North. Fig. 1 shows the orientation of the 3 accelerometers per elevation of installation. Only accelerometers 1 and 2 from each elevation are utilized in this work.

The SCADA system collects data on turbine operation, controller settings, and environmental conditions. These readings are important for pairing the behavior of the turbine to its operational status such as level of power production or the speed of incident wind flow. The yaw angle describes the orientation of the rotor relative to global North, as seen in Fig. 1. The controllers of the turbine automatically adjust the yaw angle so that the rotor and blades face towards the incoming wind.

# 2.2. Selected time-period of analysis

A time-period of 12 days is selected for analysis in which all measurement channels are continuously available, and the turbine is in normal operating conditions. Fig. 2 shows the operational conditions as measured by 3 SCADA channels (normalized between 0 and 1) for the selected time-period.

# 2.3. Data preprocessing

Prior to conducting system identification, the acceleration data readings are cleaned and preprocessed. The data is first cleaned for outliers which are removed and replaced via linear interpolation. The signals are then bandpass filtered between 0.1 and 4 Hz, which is the frequency range that includes the first few most important modes of the structure. The measurements are kept at the original sampling rate of 25 Hz.

# 3. Methods

The methods performed in this paper are organized in Fig. 3. Section 3.1 describes the automated system identification process which was performed on 10-min periods of data. Finite element (FE) modeling and model updating approaches are described in Section 3.2. For each set of

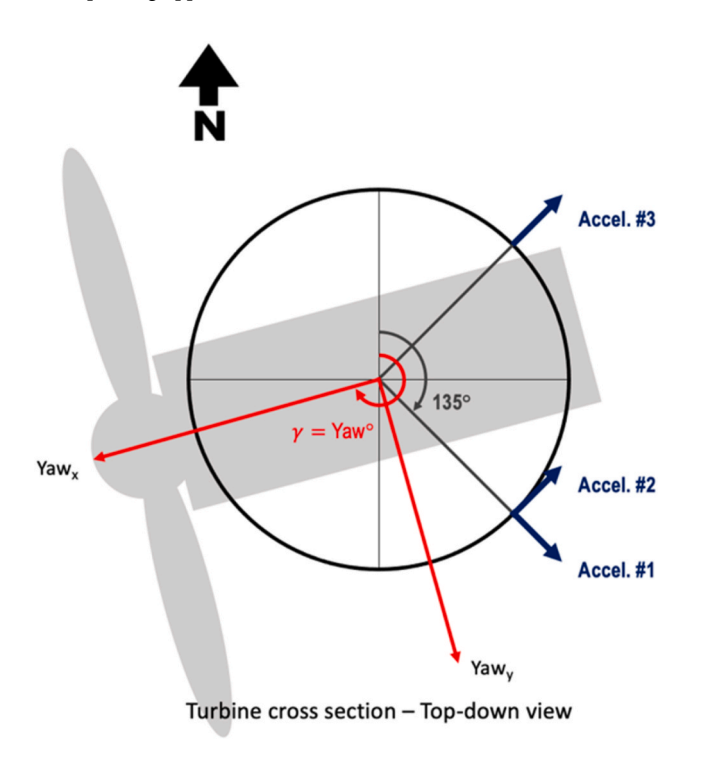


**Fig. 1.** Orientation of accelerometers at installed elevations on a cross sectional view of tower/monopile.

modal parameters obtained from system ID, an FE model of the wind turbine is updated to find an optimal set of model parameters.

#### 3.1. System identification

An automated system ID is performed on accelerometer readings from 4 elevations of the OWT to obtain modal parameters for the 1st and 2nd modes of the structure, as initial results showed that these modes contain most of the energy of the system dynamic response. This section describes the system ID methodology and the post-processing of identified modal parameters for use in model updating.

### 3.1.1. Automated stochastic subspace identification

The SSI-DATA [48] method for automated system identification is used for this analysis. This methodology provides estimates for the state space formulation of the system, from which the natural frequencies, damping ratios and mode shapes can be obtained [48,49].

The equation of motion of a discrete linear dynamic system can be written in first-order state space equation as follows:

$$\mathbf{x}_{k+1} = \mathbf{A}\mathbf{x}_k + \mathbf{B}\mathbf{u}_k + \mathbf{w}_k$$
  

$$\mathbf{y}_k = \mathbf{C}\mathbf{x}_k + \mathbf{D}\mathbf{u}_k + \mathbf{v}_k$$
(1)

where  $\mathbf{x}_k$  is the state vector,  $\mathbf{y}_k$  is the measurement vector,  $\mathbf{A}, \mathbf{B}, \mathbf{C}, \mathbf{D}$  are system, input, output and feedthrough matrices respectively.  $\mathbf{w}_k$  and  $\mathbf{v}_{k+1}$  are modeling error and measurement noise respectively. In the case the inputs are unmeasurable, effects of the inputs are included in the  $\mathbf{w}_k$  and  $\mathbf{v}_{k+1}$  terms and therefore, input and feedthrough matrices are removed from the equations. SSI-DATA is applied on output only measurements to estimate  $\mathbf{A}$  and  $\mathbf{C}$  matrices.

The estimation process of  $\mathbf{A}$  and  $\mathbf{C}$  matrices starts with forming a Hankel matrix from the measured data. By choosing a set of sensors as the reference, the reference measured data is loaded into the Hankel matrix in a block rows and b columns as the past Hankel matrix  $\mathbf{H}_p$  and the rest is loaded as the future Hankel matrix  $\mathbf{H}_f$ . The line divides the Hankel matrix into past and future parts.

$$\mathbf{H} = \frac{1}{\sqrt{\beta}} \begin{bmatrix} \mathbf{y}_{0}^{ref} & \mathbf{y}_{1}^{ref} & \cdots & \mathbf{y}_{\beta-1}^{ref} \\ \mathbf{y}_{1}^{ref} & \mathbf{y}_{2}^{ref} & \cdots & \mathbf{y}_{\beta}^{ref} \\ \vdots & \vdots & \ddots & \vdots \\ \mathbf{y}_{\alpha-1}^{ref} & \mathbf{y}_{\alpha}^{ref} & \cdots & \mathbf{y}_{\alpha+\beta-2}^{ref} \\ \mathbf{y}_{\alpha} & \mathbf{y}_{\alpha+1} & \cdots & \mathbf{y}_{\alpha+\beta-1} \\ \mathbf{y}_{\alpha+1} & \mathbf{y}_{\alpha+2} & \cdots & \mathbf{y}_{\alpha+\beta} \\ \vdots & \vdots & \ddots & \vdots \\ \mathbf{y}_{2\alpha-1} & \mathbf{y}_{2\alpha} & \cdots & \mathbf{y}_{2\alpha+\beta-2} \end{bmatrix} \end{bmatrix} \mathbf{H}_{p}$$

$$(2)$$

where ref denoted the reference sensor. Least square method can be used to predict  $\mathbf{H}_f$  using  $\mathbf{H}_p$  The least square error solution of the predicted 'future' Hankel matrix  $\mathbf{P}_a$  is [12]:

$$\mathbf{P}_{\alpha} = \mathbf{H}_{f} \mathbf{H}_{p}^{T} \left( \mathbf{H}_{p} \mathbf{H}_{p}^{T} \right)^{\dagger} \mathbf{H}_{p} \tag{3}$$

where the superscript '†' denotes pseudo-inverse operation. It was shown in Ref. [12] that  $\mathbf{P}_{\alpha}$  can be written using the observability matrix  $\mathbf{O}_{\alpha}$  and estimated state from Kalman filter  $\widehat{\mathbf{X}}_{\alpha}$ .

$$\mathbf{P}_{a} = \mathbf{O}_{a} \hat{\mathbf{X}}_{a} \tag{4}$$

Using Singular Value Decomposition (SVD) on  $\mathbf{P}_a$  from Equation (3),  $\widehat{\mathbf{X}}_a$  and  $\mathbf{O}_a$  can be estimated.

$$\mathbf{P}_{\alpha} = \underbrace{(\mathbf{U}_{n} \mathbf{\Sigma}_{n}) \left(\mathbf{\Sigma}_{n} \mathbf{V}_{n}^{T}\right)}_{\mathbf{O}_{\alpha} \qquad \hat{\mathbf{X}}_{\alpha}} \tag{5}$$

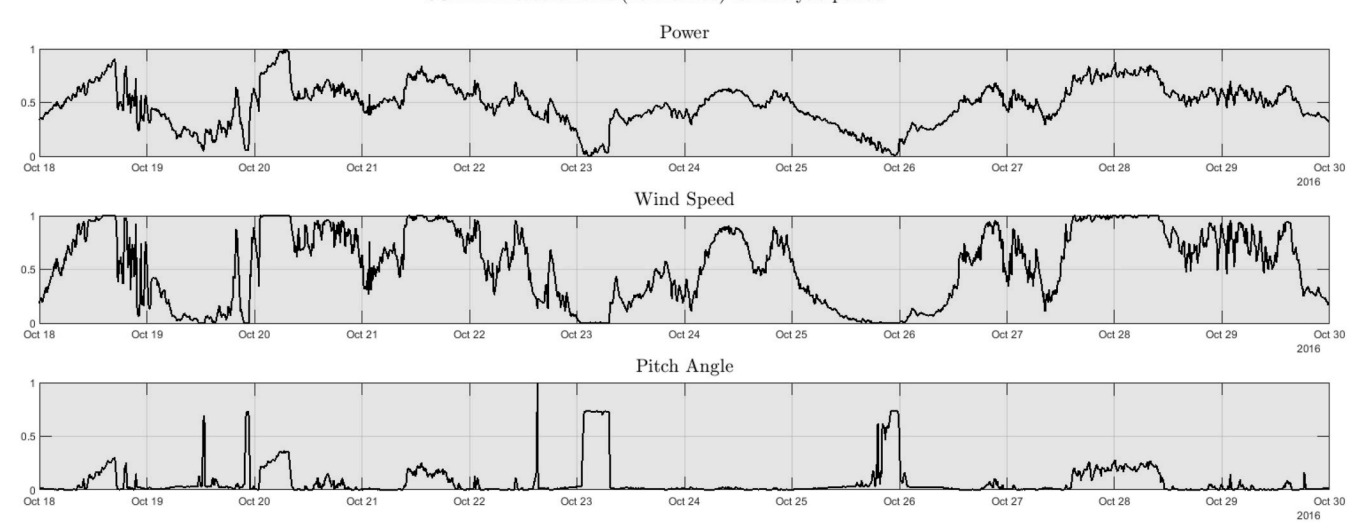


Fig. 2. SCADA system readings for 12-day period, all channels normalized.

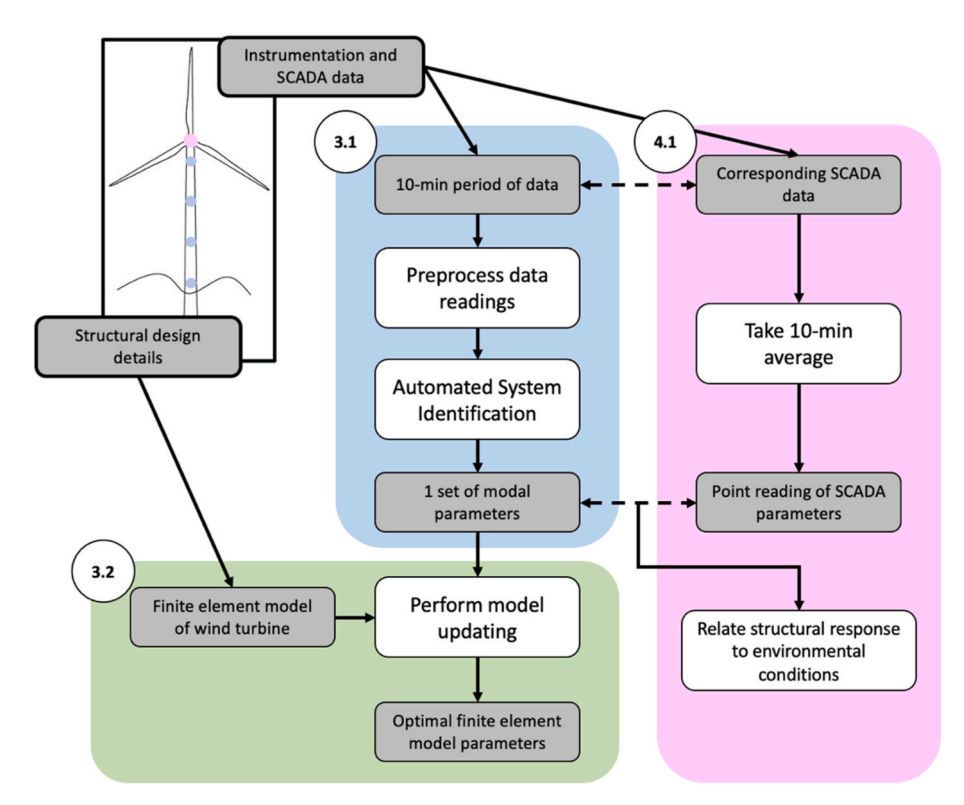


Fig. 3. Workflow, conducted on a 12-day period of operational conditions.

where n is the system order which is selected by the user. By moving the division between the past and future Hankel matrices one block row downward,  $\mathbf{H}_f^-$  and  $\mathbf{H}_p^+$  are formed. Applying the same process on these new matrices, gives an estimation for the shifted state  $\widehat{\mathbf{X}}_{\alpha+1}$ .

$$\widehat{\mathbf{X}}_{\alpha+1} = \mathbf{O}_{\alpha-1}^{\dagger} \mathbf{P}_{\alpha-1} \tag{6}$$

This way, the estimate of the system and output matrices can be given as:

$$\left[\widehat{\mathbf{X}}_{\alpha+1}\mathbf{Y}_{\alpha|\alpha}\right] = \left[\mathbf{A} \atop \mathbf{C}\right]\widehat{\mathbf{X}}_{\alpha} + \left[\mathbf{W}_{k} \atop \mathbf{V}_{k}\right] \to \left[\widehat{\mathbf{A}}\widehat{\mathbf{C}}\right] = \left[\widehat{\mathbf{X}}_{\alpha+1}\mathbf{Y}_{\alpha|\alpha}\right]\widehat{\mathbf{X}}_{\alpha}^{\dagger}$$
(7)

where  $\widehat{\mathbf{A}}$  and  $\widehat{\mathbf{C}}$  denote the estimated system matrices and  $\mathbf{Y}_{a|a}$  is the measured output at the same time step as  $\widehat{\mathbf{X}}_a$  which is the first block row of  $\mathbf{H}_f$ . Eigen value analysis is then applied on the estimated matrices to calculate the modal parameters.

In the context of continuous monitoring of structures, selecting the system order n can be challenging due to the presence of noise [50,51]. To address this, an automated process is employed, where the system order is determined based on the identification of stable modes in a stabilization diagram. In this strategy, the modal analysis is performed using different orders sequentially. In this study, a mode is considered stable if it is identified in 3 consecutive orders with less than 2% relative difference in frequencies, less than 30% relative difference in damping

ratios, and greater than 0.95 Modal Assurance Criterion (MAC) value between mode shapes. Modes with damping ratios smaller than 0 or larger than 20% are determined to be spurious and are disregarded. Finally, the smallest order which provides the maximum number of physical modes of interest is selected as the optimal order of the state space model. SSI is carried out on each 10-min set of data, providing a single set of modal parameters per dataset.

# 3.1.2. Rotation of modes

The dynamics of an OWT are generally related to the local axis of the turbine, which constantly changes as the controllers rotate the rotor to face incoming wind. Known as fore-aft (FA) and side-side (SS), these describe the coordinate directions of the structure in the local axis of an OWT. The FA direction goes through the nacelle, in line with the orientation of the rotor, while the SS direction runs orthogonal to the FA direction. As long as the controller is operating properly, the FA axis is assumed to be aligned with incoming wind.

For these reasons, we often wish to analyze modal properties of an OWT in its local axis. Mode shapes obtained from system ID describe deformation in the fixed global axis according to accelerometer installation. Thus, mode shapes are rotated into the FA and SS directions of the turbine according to its yaw angle (see Fig. 1). This allows for consistent comparison across datasets and informative insight into the behavior of the OWT.

The locations of the accelerometers are fixed on the tower at 135 deg from global North, while the yaw angle can change to any direction between 0 and 360 deg from global North. Each mode shape has components  $\phi_{45}$  and  $\phi_{135}$  which define relative deflection in the global axes 45 and 135 deg from North. These components are rotated according to the difference between the yaw angle's position and the fixed location of these axes, according to Equation (5). This provides  $\phi_x$  and  $\phi_y$ , which describe the components of modes in the local x and y axes of the OWT.

$$\begin{bmatrix} \boldsymbol{\varphi}_{x} \\ \boldsymbol{\varphi}_{y} \end{bmatrix} = \begin{bmatrix} \cos(\theta) & -\sin(\theta) \\ \sin(\theta) & \cos(\theta) \end{bmatrix} \begin{bmatrix} \boldsymbol{\varphi}_{135} \\ \boldsymbol{\varphi}_{45} \end{bmatrix}$$
(8)

where  $\theta = \gamma - 135$ , and  $\gamma$  is the yaw angle measured from global North, obtained from SCADA data. The rotation of modes is described in Fig. 4.

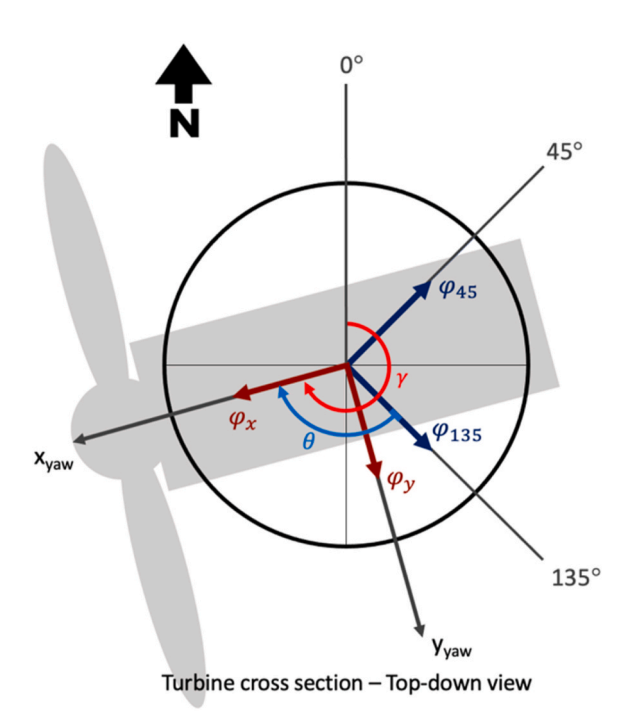


**Fig. 4.** Rotation of mode shapes from global orientation into local axis of turbine rotor.

The results are structured as one set of modal parameters for the first two identified modes of the structure for each 10-min dataset. Mode shapes have been rotated into the local axis of the turbine such that the x component of each mode shape defines deflection in the FA direction, while the y component exists in the SS direction.

#### 3.1.3. Mode identification

With all mode shapes rotated into the local axes of the turbine rotor, modes are designated as either a FA mode or a SS mode. 1st and 2nd modes of structures like an OWT typically have natural frequencies very close to each other, so modes can be identified as a FA or SS mode according to the deflected shape. Thus, modes are designated according to their MAC value with a fixed set of mode shapes used for comparison, known as reference modes. The reference mode shapes were obtained by surveying a sample of datasets for best results. The reference modes selected, seen in Fig. 5, were found to provide the clearest distinction between FA and SS deformation in the first two identified modes.

For each set of identified modal parameters, all modes in the range of the 1st and 2nd natural frequencies are isolated and then compared to the reference mode shapes. Mode shape designation is based on MAC values between identified modes and the reference mode shapes according to Equation (9). The modes with the best fit according to MAC value with each reference mode are selected as the 1st and 2nd modes of the structure, or the 1st FA and 1st SS modes.

$$MAC(\phi_{1}, \phi_{2}) = \frac{\left|\phi_{1}^{T} \phi_{2}\right|^{2}}{\phi_{1}^{T} \phi_{1} \phi_{2}^{T} \phi_{2}}$$
(9)

#### 3.2. Finite element modeling and model updating

System ID results can be used to characterize the behavior of the structure under different environmental and operational conditions. One way to leverage this information is by informing digital models of the OWT in order to improve the model's performance. In model updating, parameters of an FE model developed in OpenSees [52] are varied to find the optimal model parameters which match the modal parameters from system ID at different operating conditions.

This section describes the FE model built based on the OWT and the model updating approaches used. Deterministic model updating is carried out on each dataset of identified modal parameters and statistics of updated model parameters are studied over the entire dataset. A Bayesian approach is also used in order obtain uncertainty estimates on updated model parameters.

# 3.2.1. Initial model

The 6-MW OWT is modeled in OpenSees [52], an FE modeling software which can simulate the response of structures subjected to external loading conditions and determine modal parameters. The initial model is built using the structural design details of the tower and monopile which provide the diameter and thickness of each section, as well as the elevation and mass of platforms and other equipment in the structure. The tower and foundation are modeled as a series of linear-elastic beam column elements, each with a constant diameter and thickness. Elements vary in dimensions according to design details. Coordinate axes of the FE model are defined in Fig. 6, which shows the base of the foundation where it meets the seabed. The tower and monopile extend upwards in the positive Z direction.

In this analysis, the only soil-structure interaction information available is the macro-element stiffness matrix, composed of a lateral stiffness,  $K_{11}$ , a rotational stiffness,  $K_{22}$ , and coupled stiffness terms  $K_{12}$  and  $K_{21}$  [38]. While the soil reactions of a monopile vary with depth, at very small strains the response at the mudline can be entirely captured using the coupled macro element representation, which is shown in equation (10). The coupling of this macro element captures the influence of varying load eccentricity at the mudline level, which is the result of the depthwise varying soil subgrade moduli. The macro-element is

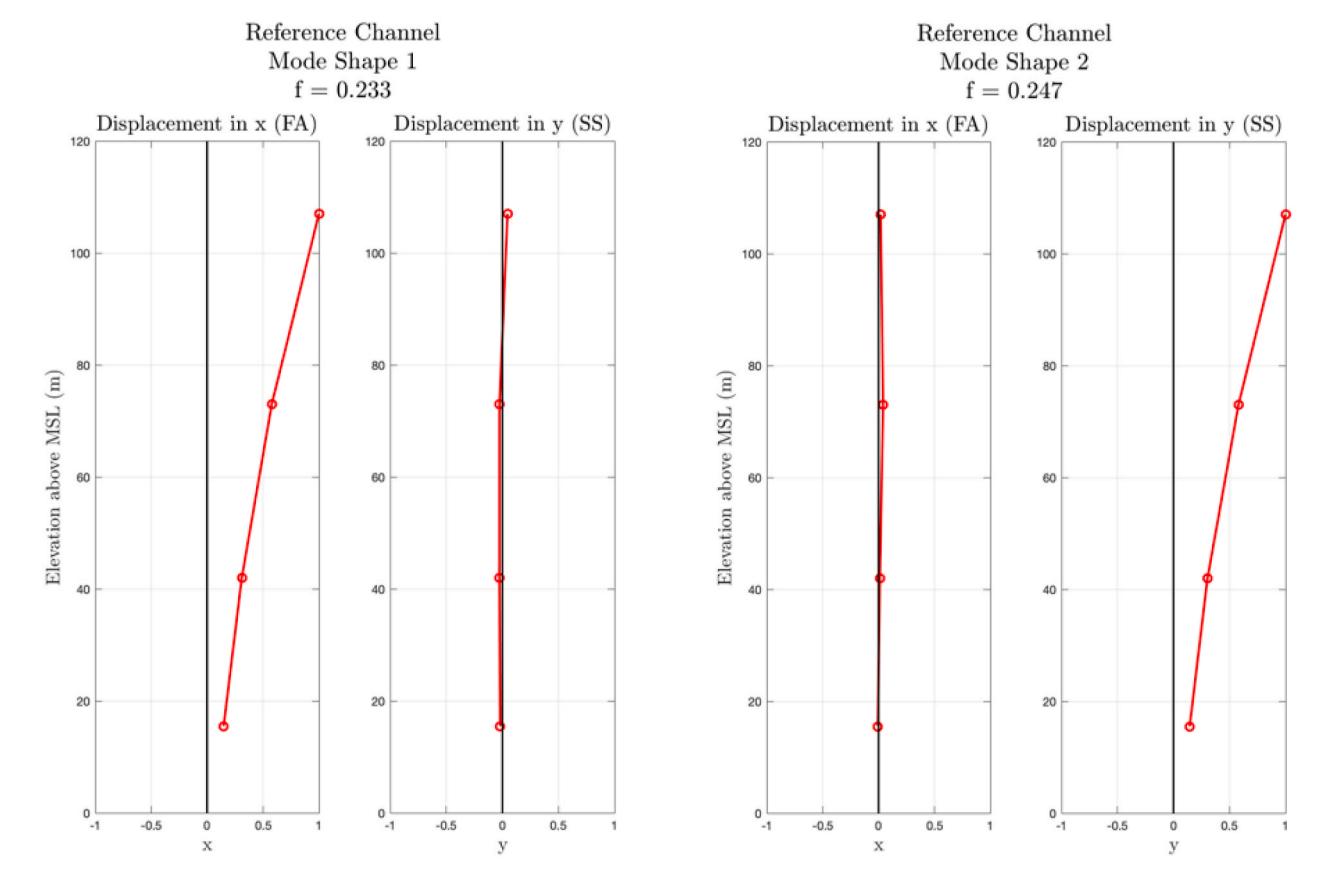


Fig. 5. Reference channel modal parameters for 1st and 2nd identified modes.

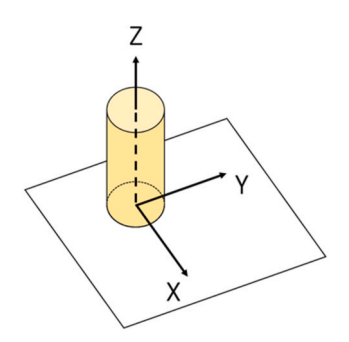


Fig. 6. Global coordinate axes of finite element model of OWT.

intended to match the soil-structure interaction while improving computational efficiency.

In our FE model, the macro-element is decomposed into equivalent lateral and rotational stiffnesses, removing the coupled terms,  $K_{12}$  and  $K_{21}.$  This is done following [37] which showed that this decomposition still produces a good match in modal parameters. The first tower mode shape corresponds to a single effective load eccentricity at the mudline, and this paper assumes that the first tower mode dominates the response and therefore simplifies the foundation model to an uncoupled representation.

$$K = \begin{bmatrix} K_{11} & K_{12} \\ K_{21} & K_{22} \end{bmatrix} \tag{10}$$

$$K_0^{lat} = \frac{K_{11}K_{22} - K_{12}^2}{K - hK_{12}} = K_X = K_Y$$
 (11)

$$K_0^{rot} = \frac{h(K_{11}K_{22} - K_{12}^2)}{hK_{11} - K_{12}} = K_{XX} = K_{YY}$$
(12)

where h is the load eccentricity and depends on the mode considered. Since we are only performing model updating for the 1st FA and SS modes, a value for h is assumed to be h=0.6H where H is the distance from the hub to the mudline of the OWT. The proportion 0.6 is chosen based on the results in Ref. [37], in which the load eccentricity for the 1st FA and SS modes was equal to approximately 60% the distance from the hub to the mudline.

Following Equations (10)–(12), the original macro-element stiffness matrix is decomposed into single lateral and rotational stiffnesses,  $K_0^{lat}$  and  $K_0^{rot}$  which are each applied in the X and Y directions at the mudline:  $K_X$ ,  $K_Y = K_0^{lat}$  and  $K_{XX}$ ,  $K_{YY} = K_0^{rot}$ . Fig. 7 depicts the decomposition of the macro-element to equivalent lateral and rotational stiffnesses applied in each direction.

A ratio, denoted R, is defined as the ratio between lateral and rotational stiffnesses affecting each direction of motion (FA and SS), computed according to  $K_0^{lat}$  and  $K_0^{rot}$  from the decomposed macroelement:

$$\frac{K_X}{K_{YY}} = \frac{K_Y}{K_{XX}} = R \tag{13}$$

The blades, hub, and nacelle are altogether referred to as the rotornacelle assembly (RNA). The mass of the RNA, its mass moment of inertia, and the location of its center of mass (CMS) are known for this OWT. The CMS is offset from the top of the tower in the vertical (Z axis) direction and in the horizontal X (FA) direction. There is no offset in the Y (SS) direction. In the FE model, the RNA is modeled as a singular lumped mass with a matrix of mass moments of inertia which is located at the CMS of the RNA and rigidly connected to the top of the tower.

Fig. 7. Macro-element stiffness matrix decomposition into equivalent lateral and rotational stiffnesses for FE model.

# 3.2.2. Deterministic model updating

In the model updating process, optimal parameters,  $\theta$ , of the FE model are found which reduce the difference between the modal parameters identified from data and by the FE model. This is accomplished through minimization of an objective function which measures the current FE modeling error in modal parameters [39], as a function of FE model parameters,  $\theta$ . Update parameters,  $\theta$ , are selected to be the lateral stiffnesses,  $K_X$  and  $K_Y$ . While these parameters vary in the optimization process,  $K_{YY}$  and  $K_{XX}$  vary accordingly following Equations (15) and (16). By keeping the ratio, R, constant, the lateral and rotational stiffnesses are always tuned by the same proportion during model updating.

$$\boldsymbol{\theta} = \begin{bmatrix} K_X \\ K_Y \end{bmatrix} = updating \ parameters \tag{14}$$

$$K_{YY} = \frac{K_X}{R} \tag{15}$$

$$K_{XX} = \frac{K_Y}{R} \tag{16}$$

The objective function for minimization is computed as a function of mode shape and natural frequency residuals between the model-predicted and data-identified modal parameters. The objective function used in this work is:

$$J(\boldsymbol{\theta}) = r(\boldsymbol{\theta})^T W_r r(\boldsymbol{\theta}) + |\boldsymbol{\theta} - \boldsymbol{\theta}_0|^T W_{\boldsymbol{\theta}} |\boldsymbol{\theta} - \boldsymbol{\theta}_0|$$
(17)

Where  $\mathbf{r}(\theta)$ , represents the residuals between the data-identified and FE model-predicted modal parameters given the current FE model parameters,  $\theta$ .  $\theta_0$  are the initial points of model parameters, and  $W_r$  and  $W_\theta$  are matrices which weight different components of  $\mathbf{r}(\theta)$  and  $\theta - \theta_0$ .

The residuals term,  $\mathbf{r}(\theta)$ , is a function of both natural frequency and mode shape residuals, or errors, and is built according to Equations (18)–(23).

$$r(\theta) = \begin{bmatrix} r_f \\ r_{\theta} \end{bmatrix} \tag{18}$$

where  $\mathbf{r}_f$  and  $\mathbf{r}_\phi$  are defined as vectors of natural frequency and mode shape residuals for each mode considered:

$$\mathbf{r}_{f} = \begin{bmatrix} e_{f}^{1} \\ e_{f}^{2} \end{bmatrix} \tag{19}$$

$$r_{\varphi} = \begin{bmatrix} e_{\varphi}^1 \\ e_{\varphi}^2 \end{bmatrix} \tag{20}$$

Where the error functions,  $e_f$  and  $\mathbf{e}_{\varphi}$ , for a given mode, m, are given by:

$$e_f^m = \frac{f_m(\boldsymbol{\theta}) - f_m(\boldsymbol{d})}{f_m(\boldsymbol{d})} \tag{21}$$

$$e_{\varphi}^{m} = \frac{\varphi_{m}(d)}{\|\varphi_{m}(d)\|} - a \frac{\varphi_{m}(\theta)}{\|\varphi_{m}(\theta)\|}$$
(22)

where a is a scaling factor given by:

$$a = \frac{\varphi_m(d)\varphi_m(\theta)}{||\varphi_m(d)|| \ ||\varphi_m(\theta)||}$$
(23)

where  $f(\theta)$  and  $\phi(\theta)$  denotes the FE model-predicted frequencies and mode shapes,  $f(\mathbf{d})$  and  $\phi(\mathbf{d})$  represent the frequencies and mode shapes obtained from system ID for the given dataset,  $\mathbf{d}$ , and m represents mode number (i.e. the FA or SS modes).

The first weight term,  $W_r$ , placed on the vector of residuals,  $\mathbf{r}(\theta)$ , is a diagonal matrix which weights the importance of each element in  $\mathbf{r}(\theta)$  based on the accuracy of different measurements/residuals or engineering judgement. The diagonal terms of this weight matrix can be selected as the inverse variance of corresponding residuals as shown in Equation (29). Weights of 5 for the frequency residuals,  $r_f$ , and 1 for the mode shape residuals,  $r_{\varphi}$ , are used following [43]. This makes the objective function more sensitive to changes in frequency error terms during optimization.

In the second weight term,  $W_{\theta}$ , a regularization is placed on the absolute difference between the current model parameters,  $\theta$ , and the starting point,  $\theta_{\theta}$ . This places a different regularization strength on each model parameter in  $\theta$ , and allows us to introduce our prior knowledge of the system into the model updating framework. System ID results (Section 4.1) show high variation in natural frequency in the FA direction which increases with wind speed, meanwhile, there is comparatively small spread in the SS frequencies. Therefore, the spring in the X (FA) direction is given a lower regularization to allow the parameter to vary more than the spring in the SS direction, reflecting the higher variation in FA frequencies intrinsic in the system.  $W_{\theta}$  is a  $2 \times 2$  diagonal matrix with the regularization weights set to 0.0005 for the spring in X and 0.005 for the spring in Y. This weight matrix is the same as the inverse covariance of prior distribution in the Bayesian framework as shown in Equation (33).

The update parameter initial points,  $\theta_0$ , are chosen using a sensitivity analysis of the FE model; they are selected as the parameter values which produce a natural frequency equal to the average frequency identified from system ID, for each direction, X (FA) and Y (SS). This is done with the aim of helping the optimization find the minimum points efficiently, by placing the starting point in the middle of the range of identified frequencies. However, the sensitivity of frequencies to changes in soil stiffness at higher frequencies (above 0.25 Hz) is very low, meaning that larger changes in stiffness are required to see changes

in the natural frequencies (Fig. 8). For this reason, when the frequency identified from system ID is above 0.25 Hz, a higher starting point is used to assist the optimization in arriving at the optimal frequency.

Before model updating is conducted, the effective young's modulus of steel, E, for the tower and monopile was changed to 220 GPa, over its original value of 200 GPa in the FE model. Fig. 8 shows the sensitivity of the first natural frequencies in the FA and SS directions with varying lateral stiffnesses, K<sub>X</sub> and K<sub>Y</sub>, for 3 different values of E. The bounds shown on the plots represent the upper and lower bounds of the FA and SS frequencies obtained in system ID. As seen in Fig. 8, an increased young's modulus of steel shifts the sensitivity plot of frequencies against soil stiffness up, resulting in higher frequencies at all stiffnesses. A shift to 220 GPa is chosen because this number allows the FE model to reach natural frequencies high enough to match the range seen in frequencies identified in the data. The larger young's modulus of steel can compensate for modeling errors such as inaccurate mass. Without this adjustment, the FE model would be unable to match the data at a certain range of frequencies. A value of 220 GPa for E also removes the need for E as its own update parameter.

The deterministic model updating framework is carried out on modal parameters obtained from each 10-min dataset in the 12-day period of analysis. This provides a single realization of optimal model parameters corresponding to each 10-min period of time. The Matlab optimization function, fminsearch, is used to perform the optimization of the objective function for each dataset. To ensure global optima are found, the objective function in the region of realistic values for  $\theta$  is investigated for a few datasets. Results show the objective function as convex in this region, with only a single minimum at the identified optimum. Optimization results are paired with corresponding 10-min average readings from the SCADA system on environmental and operational conditions. Results are shared in Section 4.2.1.

# 3.2.3. Bayesian model updating

FE model updating can also be carried out in a probabilistic manner, through Bayesian model updating. This section describes the Bayesian model updating formulation, and additional details can be found at [28, 31,53]. Let  $\theta$  represent a vector of model update parameters and let  $\boldsymbol{d}$  represent a vector of data-identified modal parameters, including natural frequencies and mode shapes. Under this framework, the posterior probability distribution  $p(\boldsymbol{d}|\theta)$  of model parameters,  $\theta$ , is estimated by invoking Bayes rule.

$$p(\boldsymbol{\theta}|\boldsymbol{d}) = \frac{p(\boldsymbol{d}|\boldsymbol{\theta})p(\boldsymbol{\theta})}{p(\boldsymbol{d})}$$
(24)

where  $p(\theta)$  is the prior distribution of FE model parameters,  $p(\boldsymbol{d}|\theta)$  —the

likelihood—is the probability distribution of the observed data given model parameters  $\theta$ , and  $p(\mathbf{d})$  is known as the evidence, or the marginal probability of the observed data,  $\mathbf{d}$ . The evidence,  $p(\mathbf{d})$ , is constant so we often simplify the above equation for the posterior probability:

$$p(\boldsymbol{\theta}|\boldsymbol{d}) = Cp(\boldsymbol{d}|\boldsymbol{\theta})p(\boldsymbol{\theta}) \propto p(\boldsymbol{d}|\boldsymbol{\theta})p(\boldsymbol{\theta})$$
(25)

Thus, we can estimate the distribution of the term  $p(\boldsymbol{d}|\theta)p(\theta)$  to obtain the location of ideal FE model parameters,  $\theta$ . The likelihood term assumes independent measurements and is formulated with the independent probabilities of modal parameters (natural frequencies and mode shapes) for some selected number of modes, M. As in the deterministic approach, the first 2 modes are selected for use in this framework, M=2.

$$p(\mathbf{d}_n|\boldsymbol{\theta}) = \prod_{m=1}^{M} p(f_m(\mathbf{d}_n)|\boldsymbol{\theta}) p(\boldsymbol{\varphi}_m(\mathbf{d}_n)|\boldsymbol{\theta})$$
(26)

To further develop the likelihood term, the errors between mode shapes and natural frequencies are modeled as a zero-mean gaussian distribution and the likelihood distribution is taken to be equal to the error distribution (with a shifted mean value). The natural frequency and mode shape errors are defined in the same way as in the deterministic approach, given in Equations (21)–(23). These terms measure the misfit between model-predicted modal parameters and those obtained from system identification, and this embeds the level of error in modal parameters into the likelihood function. By assuming these error terms follow a zero-mean Gaussian, the distribution of identified eigen frequencies and mode shapes become:

$$p(f_m(\boldsymbol{d}_n)|\boldsymbol{\theta}) \propto exp\left(-\frac{\boldsymbol{e}_f}{2\sigma_j^2}\right)$$
 (27)

$$p(\boldsymbol{\varphi}(\boldsymbol{d}_n)|\boldsymbol{\theta}) \propto exp\left(-\frac{\boldsymbol{e}_{\boldsymbol{\varphi}}}{2\sigma_n^2}\right)$$
 (28)

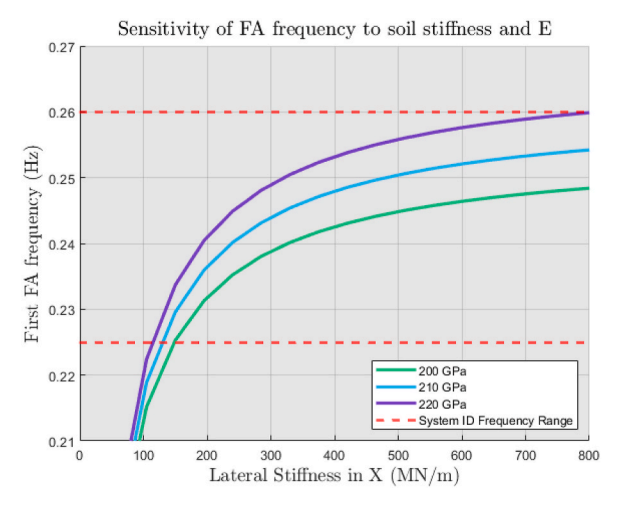
Substituting these terms into Equation (26), the likelihood term becomes:

$$p(\mathbf{d}_n|\boldsymbol{\theta}) \propto exp\left(-\frac{1}{2}J(\boldsymbol{\theta}, \boldsymbol{d})\right)$$
 (29)

where the term  $J(\boldsymbol{\theta}, \boldsymbol{d})$  is given as:

$$J(\theta, d) = \sum_{m=1}^{M} \frac{\left(e_f^m\right)^2}{\sigma_f^2} + \sum_{m=1}^{M} \frac{e_{\varphi}^{mT} e_{\varphi}^m}{\sigma_{\varphi}^2}$$
(30)

where the terms  $\sigma_f^2$  and  $\sigma_{\varphi}^2$  are selected to be aligned with the weighting



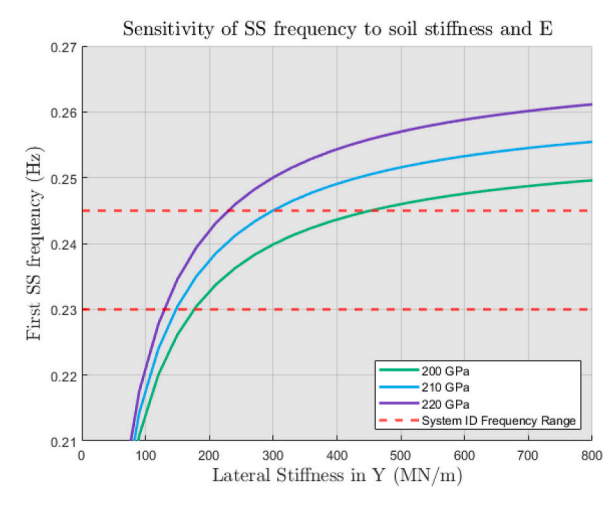


Fig. 8. FE model natural frequency sensitivity to varying soil stiffnesses for 3 values of the young's modulus of steel.

terms from the deterministic approach such that  $\frac{1}{\sigma_f^2}=5$  and  $\frac{1}{\sigma_\phi^2}=1$ . When N independent data sets exist, the likelihood and posterior become:

$$p(\mathbf{d}_{1:N}|\boldsymbol{\theta}) \propto \prod_{n=1}^{N} exp\left(-\frac{1}{2}J(\boldsymbol{\theta}, \mathbf{d}_n)\right)$$
 (31)

$$p(\boldsymbol{\theta}|\boldsymbol{d}) \propto \prod_{n=1}^{N} exp\left(-\frac{1}{2}J(\boldsymbol{\theta}, \boldsymbol{d}_n)\right) p(\boldsymbol{\theta})$$
 (32)

The prior,  $p(\theta)$ , is built based off the regularization terms used in the deterministic objective function. The prior on update parameters is assumed to be Gaussian with mean value located at the initial point,  $\theta_0$ , used in deterministic updating, and a covariance matrix equal to  $\Sigma_p = W_a^{-1}$ .

$$p(\boldsymbol{\theta}) \propto exp\left(-\frac{1}{2}|\boldsymbol{\theta} - \boldsymbol{\theta}_0|^T \boldsymbol{\Sigma}_p^{-1} |\boldsymbol{\theta} - \boldsymbol{\theta}_0|\right)$$
(33)

With this prior, the posterior from Equation (32) becomes:

$$p(\boldsymbol{\theta}|\boldsymbol{d}) \propto \prod_{n=1}^{N} exp\left(-\frac{1}{2}J(\boldsymbol{\theta}, \boldsymbol{d}_n) - \frac{1}{2}|\boldsymbol{\theta} - \boldsymbol{\theta}_0|^T \boldsymbol{\Sigma}_p^{-1}|\boldsymbol{\theta} - \boldsymbol{\theta}_0|\right)$$
(34)

The posterior distribution of model parameters is estimated through Laplace approximation [54]. This method models the posterior as a Gaussian distribution centered at the location of the maximum a posteriori (MAP) estimate—found by minimizing the negative logarithm of the posterior given by Equation (34). This posterior distribution combines information from the likelihood and the prior distributions. By comparing the minimization objective function in Equation (35) and deterministic objective function in Equation (17), we can see that the optimal model parameters,  $\theta_{\text{MAP}}$ , should fall on the mode of model parameters obtained from deterministic model updating. The location the mean of the posterior is given by:

$$\boldsymbol{\theta}_{MAP} = \underset{\boldsymbol{\theta}}{argmin} \sum_{v=1}^{N} \frac{1}{2} \left( J(\boldsymbol{\theta}, \boldsymbol{d}) + |\boldsymbol{\theta} - \boldsymbol{\theta}_{0}|^{T} \boldsymbol{W}_{\boldsymbol{\theta}} | \boldsymbol{\theta} - \boldsymbol{\theta}_{0}| \right)$$
(35)

Then, the covariance matrix on the posterior distribution is computed from the Hessian,  $H_s$  of the negative log likelihood evaluated at the mean

update value,  $J(\theta_{MAP}, d)$  as [54]:

$$\boldsymbol{\Sigma}_{\boldsymbol{\theta}}^{-1} = \frac{1}{\overline{\sigma}^2} \boldsymbol{H}_s(\boldsymbol{\theta}_{MAP}) + \boldsymbol{\Sigma}_p^{-1} \tag{36}$$

where,  $\bar{\sigma}^2 = J(\theta_{MAP},d)/[M(N_\theta+1)]$ , and  $N_\theta=2$  which is the number of update parameters [54]. Using this approach, the mean and variance of parameters  $\theta$  is estimated using all of the identified modal parameters from the 2-week period of time.

#### 4. Results

#### 4.1. System identification results

System ID results for the entire period of analysis is presented in this section. Results obtained from each 10-min dataset in the entire period include the modal parameters for the first 2 modes of the system, the 1st FA and 1st SS modes. Fig. 9 shows the 1st FA and SS natural frequencies and damping ratio of the system plotted with time, while Fig. 10 shows the same values plotted against wind speed. Wind speed is obtained by taking a 10-min average of SCADA measurements for the same time-period. Results show a correlation between the FA frequencies and damping ratios with wind speed, while the SS modal properties remain steady with increasing wind speeds or changing operational conditions. The increase in FA damping is due to aerodynamic damping [15,55], while the increase in FA frequencies is attributed to gyroscopic stiffening due to the operation of the turbine and rotation of blades.

Mode shapes for each dataset are represented in the local axis of the turbine according to the 10-min average yaw angle. Fig. 11 plots the angle that each mode makes with global North, with the yaw angle (also measured from North) overlayed for reference. Results show that the mode identified as FA is typically in very close alignment with the direction of the yaw angle, while the SS mode is oriented approximately 90° from this. These results indicate that the mode shape matching for FA/SS designation is appropriate, as it is expected that the FA mode lies in the direction of the yaw. The spread of mode shape angles could be explained by a rotor-wind misalignment in which the incident wind speed is not perfectly aligned with the FA axis of the turbine. This is due to the controller system, as the yaw angle does not begin to rotate until a large enough misalignment is measured by the SCADA system. Further, the spread is likely due in part to the 10-min window length selected in

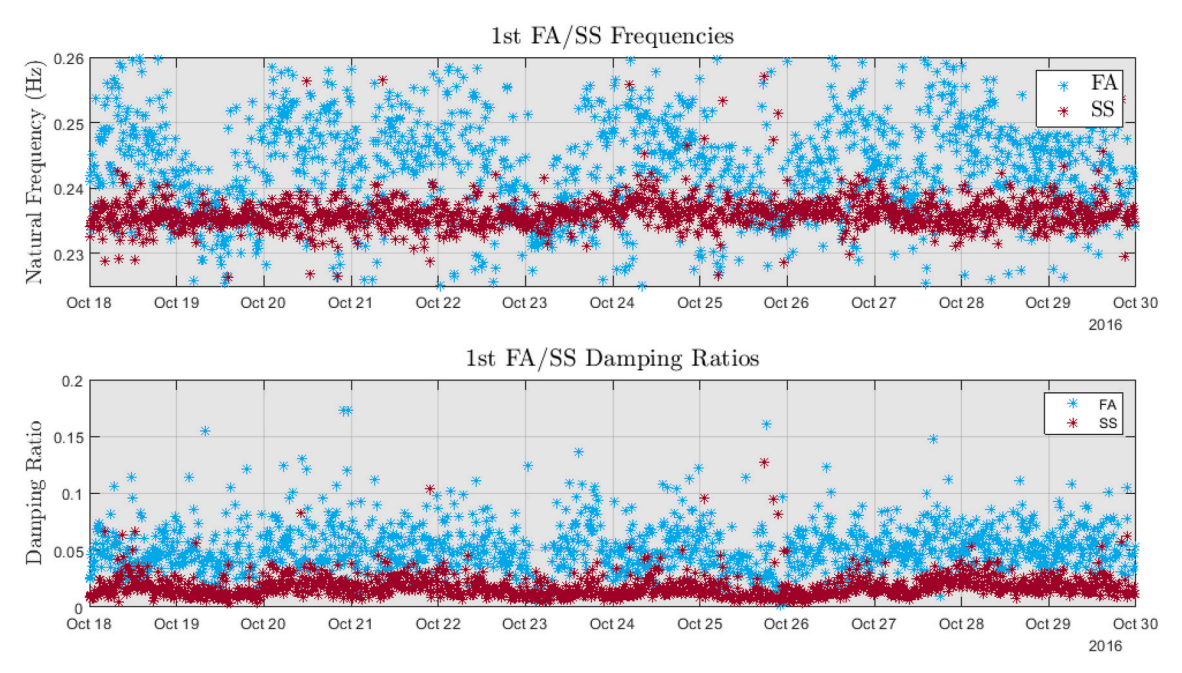


Fig. 9. First FA and SS natural frequencies (upper) and damping ratios (lower) by dataset date.

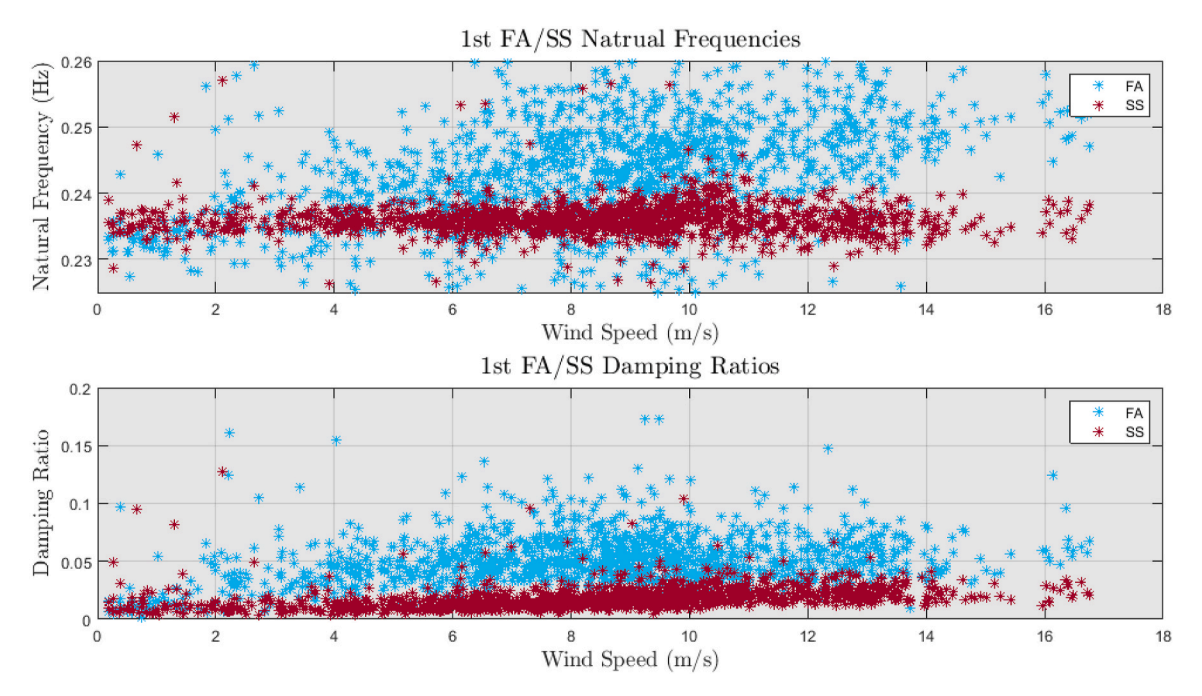
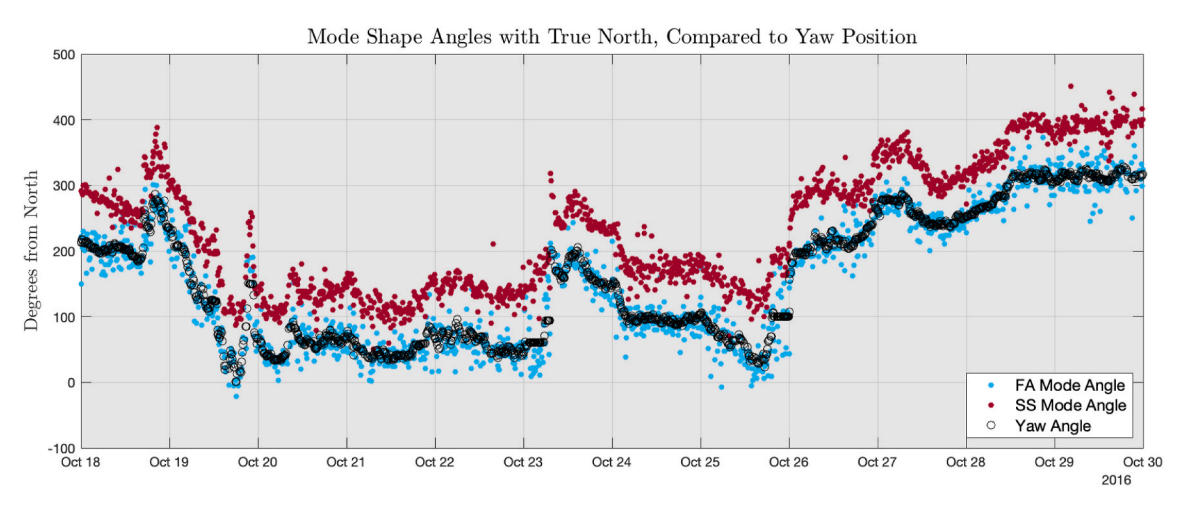


Fig. 10. First FA and SS natural frequencies (upper) and damping ratios (lower) against wind speed.



 $\textbf{Fig. 11.} \ \ \textbf{FA} \ \ \textbf{and} \ \ \textbf{SS} \ \ \textbf{mode} \ \ \textbf{shape} \ \ \textbf{angle} \ \ \textbf{with} \ \ \textbf{global} \ \ \textbf{North} \ \ \textbf{by} \ \ \textbf{dataset} \ \ \textbf{date}.$ 

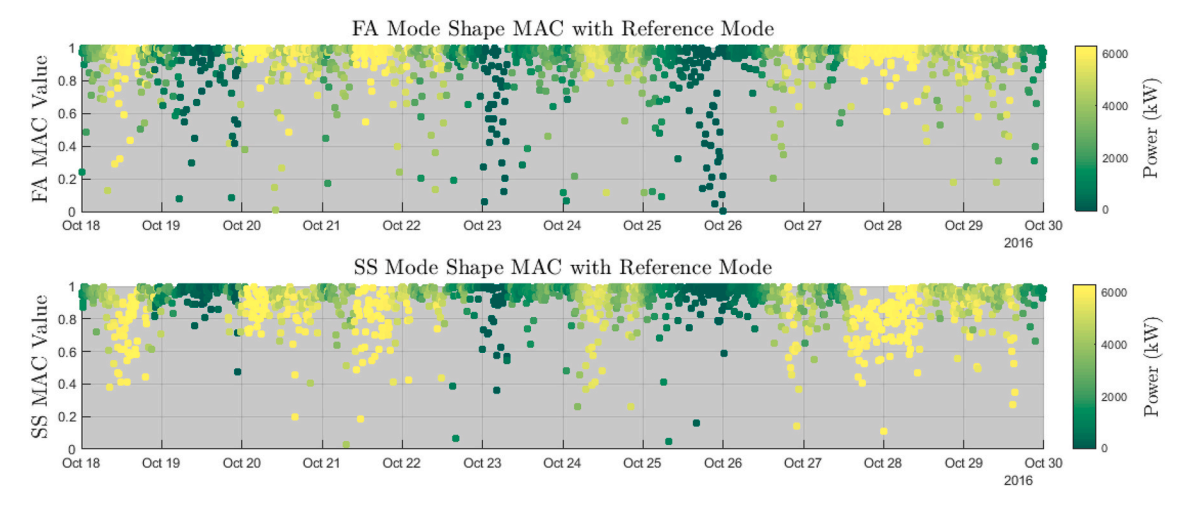


Fig. 12. FA (upper) and SS (lower) MAC value of identified modes with reference mode shape, color-coded by power output.

this work. During some 10-min periods, the yaw angle may be varying in a way which affects identified modes but cannot be captured by the 10-min average value.

MAC values of FA and SS identified modes with the corresponding reference mode are plotted against date in Fig. 12 which designates each dataset by its power output. Results show that modes typically match very well with more than 70% of FA MAC values and more than 60% of SS MAC values falling above 0.9, but there are some discrepancies during certain power conditions. Most of the lower MAC values in the FA direction occur at low power conditions. This could be explained by a lack of dynamic behavior at low wind and power conditions in which the ambient environmental conditions are not enough to excite the turbine as drastically as during operation. In the SS direction, lower MAC values are found at the max levels of power production. During the highest power conditions, the generator torque causes the strongest bending moment in the SS direction. By contrast, during lower and medium power conditions, the SS bending moments have a magnitude centered at 0. This behavior could explain the lower MAC values, as the increased torque could be changing the SS mode shapes or directions.

These patterns are further explored in Fig. 13, which shows the FA and SS MAC values plotted against the corresponding wind speed for the dataset. This figure shows that at low wind speeds, there is a consistent scatter in the FA MAC value, while at higher wind speeds, the FA MACs are concentrated at high values (with a few outliers). In the SS direction, Fig. 13 shows how the MACs at low to medium wind speeds are well concentrated at high values, but the MACs altogether drop as higher wind speeds are reached. The outliers and other inconsistencies could be due to imperfections in reference mode shapes, rotor-wind misalignment, or errors in system ID.

### 4.2. Model updating results

# 4.2.1. Deterministic model updating

Results from the deterministic model updating approach are provided in this section. For each 10-min dataset, 1 set of optimal modal parameters (lateral stiffnesses in X and Y:  $K_X$ ,  $K_Y$ ) which minimize the FE model residuals with the data are obtained. Fig. 14 shows the resulting natural frequencies of the updated models against wind speed, plotted next to the system ID obtained frequencies for comparison. Overall trends with wind speed match well. Fig. 15 shows the fit between model updated frequencies and their corresponding frequencies identified in system ID for each dataset in the time period of analysis.

Fig. 16 shows the absolute error in FA and SS frequencies between updated models and data. The mean absolute error in both the FA and SS are below  $0.01~\mathrm{Hz}$ , and the distribution of errors is approximately normally distributed around 0, indicating no consistent over- or underestimation of natural frequencies.

Fig. 17 shows the optimal lateral soil stiffnesses in the X (FA) and Y (SS) directions after model updating, plotted against the corresponding wind speed from SCADA data for each dataset. Due to increasing frequencies in the FA direction, the effective FA lateral stiffness at the mudline increases with wind speed, while the effective SS lateral stiffness remains constant with changing operational conditions. While the soil stiffnesses themselves do not change, our model updating framework is intended to capture the effective changes in stiffness as a function of operational conditions. The FA lateral stiffness increase is due to an unmodeled effect (gyroscopic stiffening) causing an increase in natural frequencies with higher wind speeds.

# 4.2.2. Bayesian model updating

Fig. 18 shows the posterior probability distribution of update parameters based on the estimates of the mean and covariance of update parameters,  $\theta$ . Posterior estimates are shown considering 100 datasets, 500 datasets, and all (1384) datasets. The underlying histogram represents the update values obtained from deterministic model updating, a frequentist counterpart of model parameter probability distributions. The goal in Bayesian updating was to obtain a mean estimate for a single set of optimal model parameters—which would fall at the mode of the frequentist results—and a variance which represents the uncertainty in the estimation.

Results show that the location of optimal parameters falls close to the mode of the histogram of results obtained in the frequentist approach. As more datasets of modal parameters are considered, the variance of the marginal posterior distributions decrease, showing how the information gained by the inclusion of more datasets increases the certainty in this estimation. This is expected as shown in previous studies by Ref. [31]. The Bayesian approach to model updating successfully identifies the location of optimal model parameters with high certainty, however, this method does not consider the inherent variability that modal parameters have with environmental conditions like wind speed.

### 5. Conclusions

This paper carried out automated system identification and model

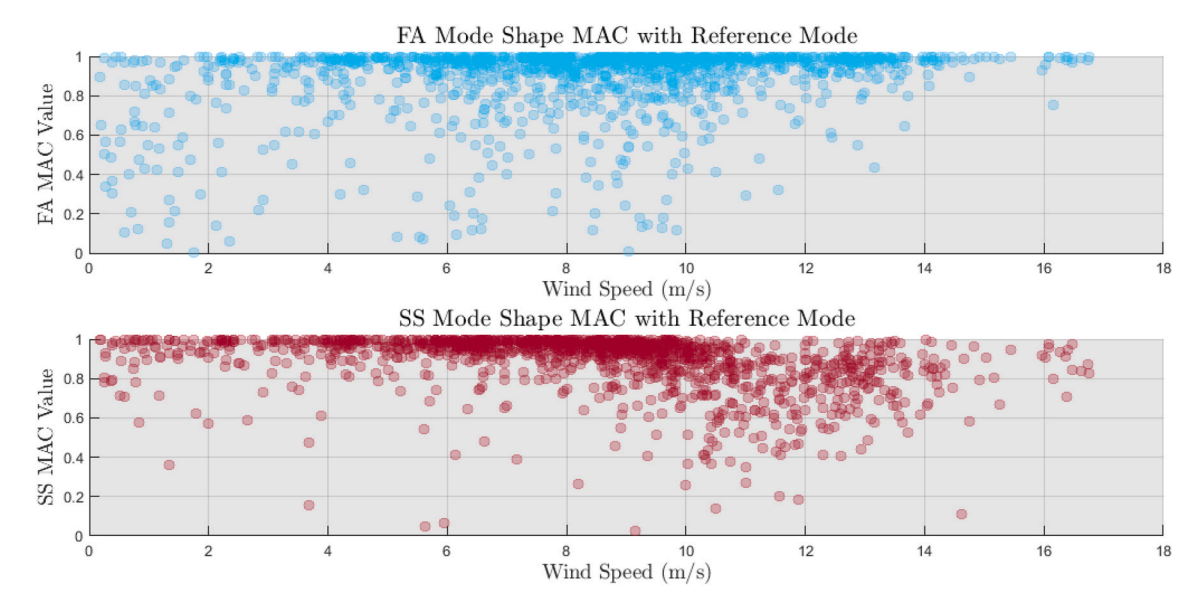


Fig. 13. FA (upper) and SS (lower) MAC values with reference mode shapes, plotted against wind speed.

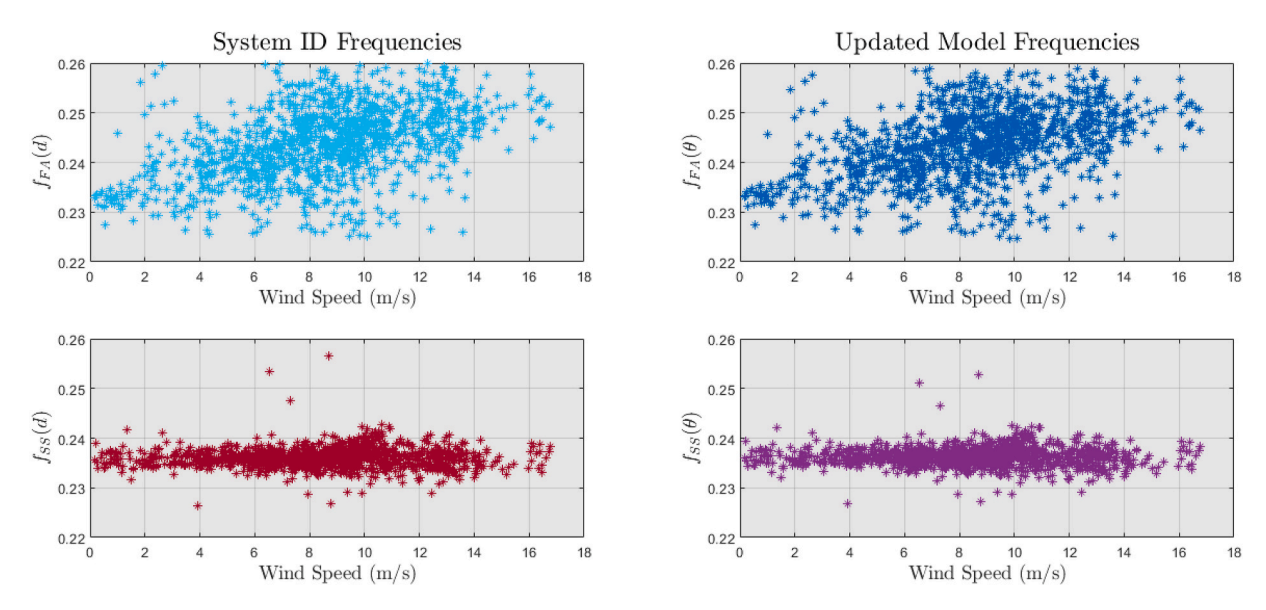


Fig. 14. System ID (left) and updated model (right) natural frequencies (FA on top, SS on bottom) compared against wind speed.

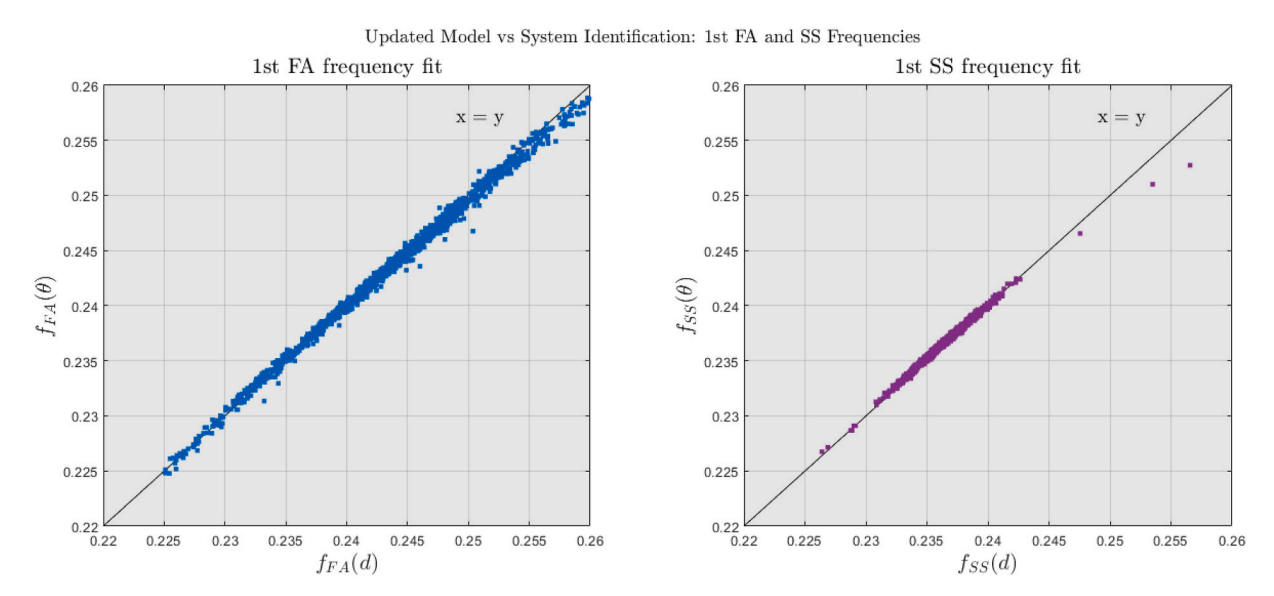


Fig. 15. Fit between updated model 1st FA (left) and SS (right) natural frequencies and identified frequencies from system ID.

updating of an operational 6 MW OWT. Automated SSI-DATA was used to extract modal parameters for the first 2 modes—the 1st FA and 1st SS mode—from instrumented accelerometers over two weeks of operation. Modal properties are paired with corresponding SCADA data which tracks wind speed and power output. Results show an increase in the 1st FA natural frequency and damping ratio with increasing wind speed, attributed to gyroscopic stiffening due to the operation of the OWT.

An FE model of the OWT was built in OpenSees based on design information for the monopile and tower with a lumped mass at the tower-top to represent the RNA. The macro-element for soil-structure interaction at the mudline was decomposed into equivalent lateral and rotational stiffnesses which are each applied in the X (FA) and Y (SS) directions of the FE model. Extracted modal parameters were used in 2 methods for FE model updating in which the lateral stiffnesses in X and Y are used as update parameters while the rotational stiffnesses vary according to a fixed ratio. The deterministic update resulted in 1 realization of optimal model parameters per dataset (each representing 10 min of data), which were assessed against wind speed. Results showed a small mean absolute error (MAE) between updated model and identified

natural frequencies. Gyroscopic effects which cause an increase in the FA frequencies with wind speed were captured in the updated effective soil spring stiffnesses at the mudline, reflected by an increase in soil stiffness in the FA direction with wind speed.

The Bayesian model updating approach provides a posterior probability distribution for the model parameters given the datasets provided. The optimal model parameters and their estimation uncertainty can be obtained as the mode and standard deviation of marginal parameter distributions. Posterior distribution estimations are compared for a varying number of datasets used to inform the likelihood distribution. Results show that the posterior distribution becomes narrower with smaller standard deviation on parameter estimates as more data is considered.

Given the intrinsic variation with environmental conditions observed in system identification results, the next step of this work will be to conduct a Hierarchical Bayesian model updating which would allow us to consider an underlying variability in model parameters [56]. This variability can be estimated as hyperparameter and is expected to match the shape of the frequentist approach. Future modeling will also

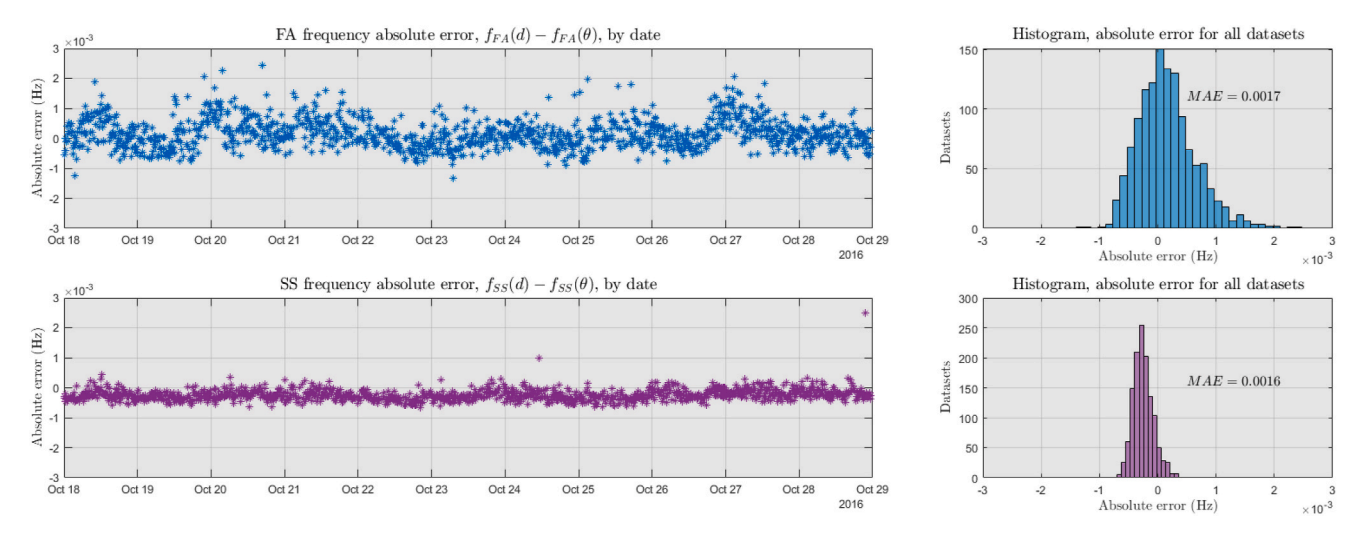


Fig. 16. Absolute error in updated model 1st FA (upper) and SS (lower) natural frequencies.

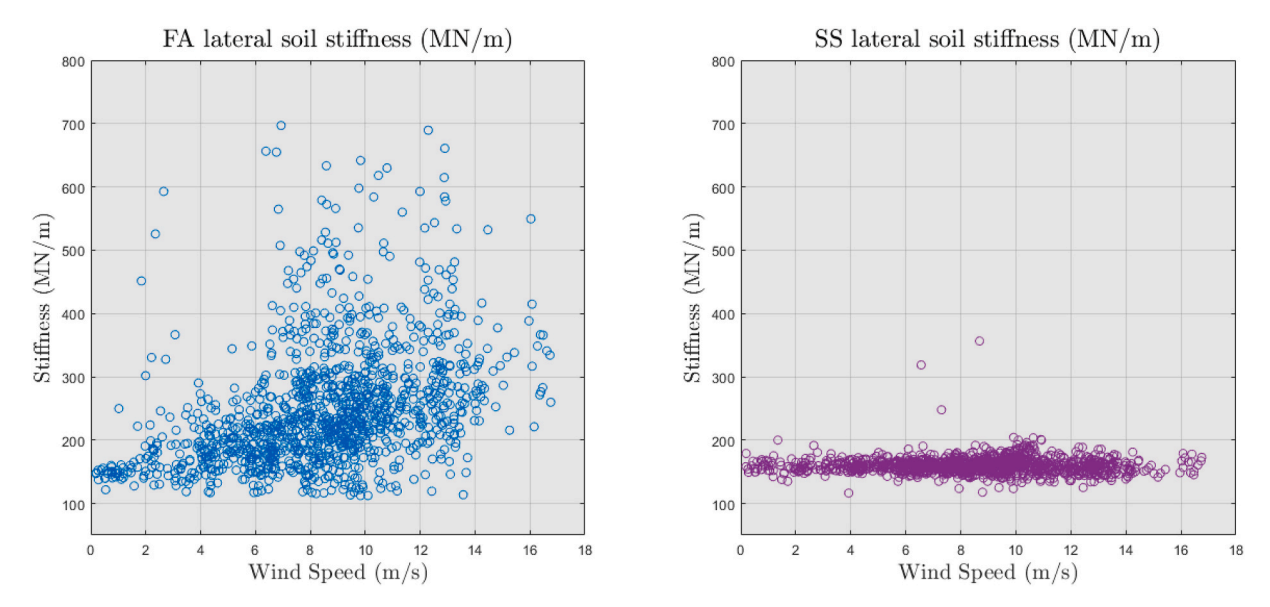


Fig. 17. Updated model effective lateral soil stiffness in FA (left) and SS (right) directions against wind speed.

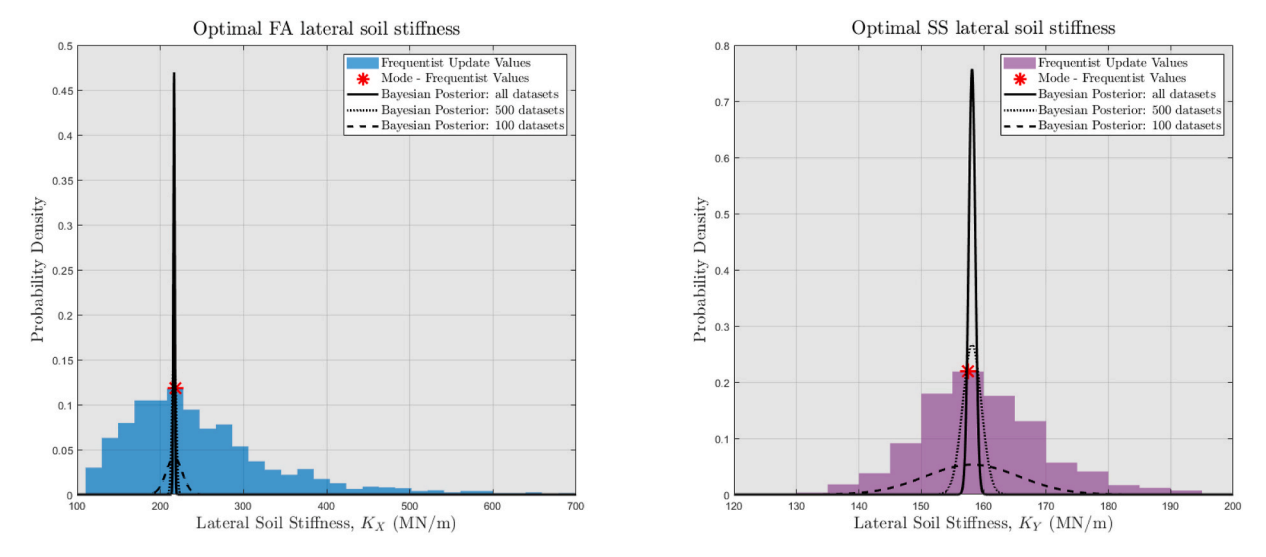


Fig. 18. Bayesian model update posterior distribution of update parameters.

need to directly model the effect of gyroscopic stiffening at the hub level so that soil springs values are not required to compensate for the gyroscopic stiffening.

# 6 Data Accessibility

Data used in this work is under NDA and is not available to be shared.

#### CRediT authorship contribution statement

**Bridget Moynihan:** Conceptualization, Methodology, Formal analysis, Writing – original draft. **Azin Mehrjoo:** Methodology, Formal analysis, Writing – original draft. **Babak Moaveni:** Conceptualization, Writing – review & editing. **Ross McAdam:** Writing – review & editing, Supervision. **Finn Rüdinger:** Writing – review & editing, Supervision. **Eric Hines:** Writing – review & editing, Supervision.

# Declaration of competing interest

The authors declare that they have no known competing financial interests or personal relationships that could have appeared to influence the work reported in this paper.

#### Acknowledgements

The authors acknowledge partial support of this study by the National Science Foundation grant 2230630. Opinions, findings, and conclusions expressed in this paper are those of the authors and do not necessarily represent the views of the sponsors and organizations involved in this project.

#### References

- [1] W. Musial, P. Spitsen, P. Duffy, P. Beiter, M. Marquis, R. Hammond, M. Shields, Offshore Wind Market Report, 2022 Edition, U.S. Department of Energy, 2022.
- [2] M. Shields, J. Stefek, F. Oteri, M. Kreider, E. Gill, S. Maniak, R. Gould, C. Malvik, S. Tirone, E. Hines, A Supply Chain Road Map for Offshore Wind Energy in the United States, National Renewable Energy Laboratory (NREL), Golden, CO, 2023.
- [3] P. G. M. W. Z. L. G. K. S. F. A. I. W. L. Jiaxuan Leng, Condition-based structural health monitoring of offshore wind jacket structures: opportunities, challenges, and perspectives, Struct. Health Monit. (2023).
- [4] D. McMillan, G.W. Ault, Quantification of condition monitoring benefit for, Wind Eng. 31 (4) (2007) 267–285.
- [5] I. Antoniadou, N. Dervilis, E. Papatheou, A. Maguire, K. Worden, Aspects of structural health and condition monitoring of offshore wind turbines, Philosophical Transactions of the Royal Society A 373 (2035) (2015).
- [6] A. Moreno-Gomez, C.A. Perez-Ramirez, A. Dominguez-Gonzalez, M. Valtierra-Rodriguez, O. Chavez-Alegria, J.P. Amezquita-Sanchez, Sensors used in structural health monitoring, Arch. Comput. Methods Eng. 25 (2018) 901–918.
- [7] D. Goyal, B. Pabla, The vibration monitoring methods and signal processing techniques for structural health monitoring: a review, Arch. Comput. Methods Eng. 23 (2016) 585–594.
- [8] A. Mehrjoo, M. Song, B. Moaveni, C. Papadimitriou, E. Hines, Optimal sensor placement for parameter estimation and virtual sensing of strains on an offshore wind turbine considering sensor installation cost, Mech. Syst. Signal Process. 169 (2022).
- [9] H.-N. Li, L. Ren, Z.-G. Jia, T.-H. Yi, D.-S. Li, State-of-the-art in structural health monitoring of large and complex civil infrastructures, Journal of Civil Structural Health Monitoring 6 (2016) 3–16.
- [10] C.R. Farrar, K. Worden, An introduction to structural health monitoring, Philosophical Transactions of the Royal Society A 365 (1851) (2006).
- [11] P. Moser, B. Moaveni, Environmental effects on the identified natural frequencies of the Dowling Hall Footbridge, Mech. Syst. Signal Process. 25 (7) (2011) 2336–2357.
- [12] P. Van Overschee, B. De Moor, Subspace Identification for Linear Systems: Theory—Implementation—Applications, Springs Science & Business Media, Dec 6 2012.
- [13] B. Peeters and G. De Roeck, "Reference-based stochastic subspace identification for output-only modal analysis," Mech. Syst. Signal Process., vol. 16, no. 6, pp. 855-878.
- [14] E.M. Hines, C.D. Baxter, D. Ciochetto, M. Song, P. Sparrevik, H.J. Meland, J. M. Strout, A. Bradshaw, S. Hu, J.R. Basurto, B. Moaveni, Structural instrumentation and monitoring of the block island offshore wind farm, Renew. Energy 202 (2023) 1032–1045.
- [15] N. Partovi-Mehr, E. Branlard, M. Song, B. Moaveni and E. Hines, "Modeling of an Offshore Wind Turbine and Sensitivity Analysis of its Dynamic Properties to

- Operational and Environmental Conditions," Available at: SSRN: https://ssrn.com/abstract=4312852.
- [16] T. Chan, Z. Li, Y. Yu, Z. Sun, Concurrent multi-scale modeling of civil infrastructures for analyses on structural deteriorating—Part II: model updating and verification, Finite Elem. Anal. Des. 45 (11) (2009) 795–805.
- [17] J. Brownjohn, P. Moyo, P. Omenzetter, Y. Lu, Assessment of highway bridge upgrading by dynamic desting and finite-element model udpating, J. Bridge Eng. 8 (2003) 162–172.
- [18] A. Teughels, G. De Roeck, Structural damage identification of the highway bridge Z24 by FE model updating, J. Sound Vib. 278 (2004) 589–610.
- [19] E. Reynders, G. De Roeck, P. Grundes Bakir, C. Sauvage, Damage identification of the Tilff Bridge by vibration monitoring using optical fiber strain sensors, J. Eng. Mech. 133 (2007) 185–193.
- [20] S. Fang, R. Perera, G. De Roeck, Damage identification of a reinforced concrete frame by finite element model updating using damage parameterization, J. Sound Vib. 313 (2008) 544–559.
- [21] M. Song, S. Yousefianmoghadam, M.-E. Mohammadi, B. Moaveni, A. Stavridis, R. L. Wood, An application of finite element model updating for damage assessment of a two-story reinforced concrete building and comparison with lidar, Struct. Health Monit. 17 (5) (2017).
- [22] A. Nozari, I. Behmanesh, S. Yousefianmoghadam, B. Moaveni, A. Stavridis, Effects of variability in ambient vibration data on model updating and damage identification of a 10-story building, Eng. Struct. 151 (2017) 540–553.
- [23] A. Nozari, S. Bose, B. Moaveni, A. Stavridis, Finite element model updating and damage identification of a school building in Sankhu, Nepal, Condition Monitoring and Performance Degradation of Civil Structures Including Fatigue Effects on Offshore Wind Turbine Support Structures (2020) 82.
- [24] S. Ereiz, I. Duvnjak, J.F. Jimenez-Alonso, Review of finite element model updating methods for structural applications, Structures 41 (2022) 684–723.
- [25] J. Beck, L. Katafygiotis, Updating models and their uncertainties. I: bayesian statistical framework, J. Eng. Mech. 124 (4) (1998).
- [26] K.-V. Yuen, Bayesian Methods for Structural Dynamics and Civil Engineering, John Wiley & Sons, 2010.
- [27] E. Simoen, G. De Roeck, G. Lombaert, Dealing with uncertainty in model updating for damage assessment: a review, Mech. Syst. Signal Process. 56 (2015) 123–149.
- [28] M. Song, L. Renson, N. jean-Philippe, B. Moaveni, G. Kerschen, Bayesian model updating of nonlinear systems using nonlinear normal modes, Struct. Control Health Monit. 25 (12) (2018).
- [29] G. Sevieri, M. Andreini, A. De Falco, H. Matthies, Concrete gravity dams model parameters updating using static measurements, Eng. Struct. 196 (2019).
- [30] M. Song, B. Moaveni, C. Papadimitriou, A. Stavridis, Accounting for amplitude of excitation in model updating through a hierarchical Bayesian approach: application to a two-story reinforced concrete building, Mech. Syst. Signal Process. 123 (2019) 68–83.
- [31] I. Behmanesh, B. Moaveni, Probabilistic identification of simulated damage on the Dowling Hall footbridge through Bayesian finite element model updating, Struct. Control Health Monit. 22 (3) (2014) 463–483.
- [32] Y. Huang, C. Shao, B. Wu, J.L. Beck, H. Li, State-of-the-art review on Bayesian inference in structural system identification and damage assessment, Adv. Struct. Eng. 22 (6) (2018).
- [33] m. Muto, J.L. Beck, Bayesian updating and model class selection for hysteretic structural models using stochastic simulation, J. Vib. Control 14 (1–2) (2008).
- [34] B. Fitzgerald, D. Igoe, S. Sarkar, A comparison of soil structure interaction models for dynamic analysis of offshore wind turbines, in: The Science of Making Torque from Wind, TORQUE), 2020.
- [35] K. Sunday, F. Brennan, Influence of soil-structure modelling techniques on offshore wind turbine monopile structural response, Wind Energy 25 (6) (2022) 998–1012.
- [36] I.B. Loken, A.M. Kaynia, Effect of foundation type and modelling on dynamic response and fatigue of offshore wind turbines, Wind Energy 22 (12) (2019).
- [37] R.A. McAdam, M.N. Chatzis, M. Kuleli, E. Anderson, B.W. Byrne, Foundation stiffness estimation of an instrumented offshore wind turbine through model updating, Review (2023).
- [38] A.M. Page, G. Grimstad, G. Reider Eiksund, H. Petter Jostad, A macro-element pile foundation model for integrated analyses of monopile-based offshore wind turbiens, Ocean. Eng. 167 (2018) 23–35.
- [39] Z. Zhang, C. Sun, V. Jahangiri, Structural damage identification of offshore wind turbines: a two-step strategy via FE model updating, Struct. Control Health Monit. 29 (2) (2021).
- [40] Y. Xu, G. Nikitas, T. Zhang, Q. Han, M. Chryssanthopoulos, S. Battacharya, Y. Wang, Support condition monitoring of offshore wind turbines using model updating techniques, Struct. Health Monit. 19 (4) (2019) 1017–1031.
- [41] S. Cong, S.-L.J. Hu, H.-J. Li, Using incomplete complex modes for model updating of monopiled offshore wind turbines, Renew. Energy 181 (2022) 522–534.
- [42] K. Schroder, C.G. Gebhardt, R. Rolfes, A two-step appraoch to damage localization at supporting structures of offshore wind turbines, Struct. Health Monit. 17 (5) (2018) 1313–1330.
- [43] M.-S. Nabiyan, F. Khoshnoudian, B. Moaveni, H. Ebrahimian, Mechanics-based model updating for identification and virtual sensing of an offshore wind turbine using sparse measurements, Struct. Control Health Monit. 28 (2) (2020).
- [44] M. Song, B. Moaveni, H. Ebrahimian, E. Hines, A. Bajric, Joint parameter-input estimation for digital twinning of the Block Island wind turbine using output-only measurements, Mech. Syst. Signal Process. 198 (2023).
- [45] D. Augustyn, U. Smolka, U.T. Tygesen, M.D. Ulriksen, J.D. Sorensen, Data-driven model updating of an offshore wind jacket substructure, Appl. Ocean Res. 104 (2020).

- [46] P. Xu, J. Chen, J. Li, S. Fan, Q. Xu, Using Bayesian updating for monopile offshore
- wind turbines monitoring, Ocean. Eng. 280 (2023).
  "Our offshore wind farms," Ørsted, [Online]. Available: https://orsted.com/en/ourbusiness/offshore-wind/our-offshore-wind-farms.
- [48] P. van Overschee, B. De Moor, Subspace Identification for Linear Systems, Kluwer Academic Publishers, 1996.
- [49] R. Brincker, P. Andersen, Understanding Stochastic Subspace Identification, 2006.
- [50] C. Priori, M. De Angelis, R. Betti, On the selection of user-defined parameters in data-driven stochastic subspace identification, Mech. Syst. Signal Process. 100 (2018) 501-523.
- [51] E. Tronci, M. De Angelis, R. Betti, V. Altomare, Semi-automated operational modal analysis methodology to optimize modal parameter estimation, J. Optim. Theor. Appl. 187 (2020) 842-854.
- [52] OpenSees [Online]. Available: https://opensees.berkeley.edu/.
- [53] J.L. Beck, S.-K. Au, Bayesian model updating of nonlinear systems using nonlinear normal modes, J. Eng. Mech. 128 (4) (2002).
- [54] B. Bagirgan, A. Mehrjoo, B. Moaveni, C. Papadimitriou, U. Khan, J. Rife, Iterative optimal sensor placement for adaptive structural identification using mobile sensors: numerical application to a footbridge, Mech. Syst. Signal Process. 200 (2023).
- [55] X. Liu, C. Lu, G. Li, A. Godbole, Y. Chen, Effects of aerodynamic damping on the tower load of offshore horizontal axis wind turbines, Appl. Energy 204 (2017)
- [56] I. Behmanesh, B. Moaveni, G. Lombaert, C. Papadimitriou, Hierarchical Bayesian model updating for structural identification, Mech. Syst. Signal Process. (2015) 360–376.